SAND2005-7696C

Experimental Investigation of Oxidation Processes in a Swirl-Supported Diesel Engine

Paul C. Miles*
Sandia National Laboratories

Robert Collin, Leif Hildingsson, and Anders Hultqvist
Lund Institute of Technology

Öivind Andersson
Volvo Car Corporation

* Corresponding author: PO Box 969, MS9053
Livermore, CA 94551-0969 USA
e-mail: pcmiles@sandia.gov
phone: 1 925 294 1512
fax: 1 925 294 1004

Keywords: *Diesel engines, turbulent flows, soot, diagnostics*

Word Count (Method 1):

Main Text:	3638
References: (10+2) x 2.3 x 7.6	210
Table 1: (15+2) x 7.6 x 1 col.	129
Fig. 1: (93+10) x 2.2 x 1 col. + 12	239
Fig. 2: (74+10) x 2.2 x 1 col. + 32	217
Fig. 3: (43+10) x 2.2 x 1 col. + 15	132
Fig. 4: (59+10) x 2.2 x 1 col. + 48	200
Fig. 5: (69+10) x 2.2 x 2 col. + 29	377
Fig. 6: (76+10) x 2.2 x 2 col. + 32	410
Fig. 7: (71+10) x 2.2 x 1 col. + 26	204
Total:	5756

Abstract

The evolution of bulk flow structures and their interaction with the spatial distribution of heat release zones and of partially-oxidized fuel and particulate matter is examined experimentally in a swirl-supported, direct-injection diesel engine. Vector fields describing the bulk flow structures are measured with particle image velocimetry (PIV), while complementary scalar field measurements of partially-oxidized fuel and particulates are obtained in the same vertical plane using broadband laser-induced fluorescence (LIF) and laser-induced incandescence (LII) techniques, respectively. The two-dimensional divergence of the mean velocity fields is also employed to provide information on the mean locations of heat release. Measurements are performed at a highly-dilute, 12% O_2, operating condition characteristic of low-NO_x, low-temperature diesel combustion systems. The spatial distributions of unburned fuel rapidly develop a structure characterized by two separate zones of high fuel concentration, an inner zone in the cylinder center and an outer zone in the squish volume. Single-cycle measurements show that this two-zone structure is present on an individual cycle basis, and is not an artifact of averaging distinct, single-zone distributions. For this engine build, the mean flow structures developed do not actively promote mixing of either zone, although bulk flow structures in the upper-central region of the cylinder vary significantly on a cycle-by-cycle basis. The measured spatial distributions of particulates indicate that particulates are formed primarily in the inner zone—and remain un-oxidized late in the cycle.

1. Introduction

Due to the high thermal efficiency of diesel engines, increasing their use in the personal transportation sector can result in significant reductions in both energy consumption and

CO_2 emissions. However, both current and future vehicle emissions standards are extremely difficult to meet with conventional diesel engine technology, due to the high emissions of both NO_x and particulate matter (soot). Low-temperature combustion strategies have recently been proposed to reduce NO_x emissions without unduly prejudicing soot emissions (*e.g.* [1], [2]). These strategies generally rely on either high-dilution (to lower the $[O_2]$ in the intake charge) or late combustion phasing (to take advantage of expansion cooling) to keep peak combustion temperatures low. In both cases, mixing of the fuel with sufficient oxidizer becomes increasingly difficult, due either to the increased volume of ambient fluid required or to the reduced time available. Insufficient fuel-air mixing leads to increased soot (and CO) emissions as well as reduced fuel economy.

Mixing in direct-injection diesel engines is influenced by both fuel injection parameters (injection pressure, hole-size, *etc.*) and by the later transport of partially-mixed fuel by bulk flow structures, which also serve to generate turbulence to enhance the small-scale mixing. Reliance on this later mixing is particularly pronounced for light-duty, automotive-sector diesels. Numerical simulations of the combustion process in these engines indicate that, under appropriate conditions, beneficial flow structures that correlate well with measured increases in late-cycle heat release rates can be formed [3]. However, direct experimental confirmation of the formation of these structures, and their influence on the spatial distribution and burn-out of partially-oxidized fuel and soot, has not been previously achieved. Although spatial distributions of unburned fuel and soot have been measured in both heavy-duty (*e.g.* [4], [5]) and light-duty engines ([6], [7]), the in-cylinder flow structures have eluded experimental observation. Hence, the joint

experimental description of the velocity and scalar fields contained herein is unique, and represents a significant advancement in our ability to evaluate the accuracy of numerical simulations and to understand phenomenologically the development of the combustion process. Additionally, full-field measurements realized on a single-cycle basis permit assessment of the degree to which the mean flow and scalar fields represent the individual cycle fields, and assessment of whether or not modeling approaches providing more information than is provided by Reynolds-averaged approaches will be required to capture real engine behavior.

2. Engine Facility and Experimental Set-up

The experiments were conducted in a direct-injection diesel engine based on the Volvo D5, a light-duty engine characterized by an 81 mm bore and a single-cylinder displacement of 480 cm^3. The production bowl geometry has been modified to facilitate planar imaging within the bowl while retaining the dominant features of a realistic bowl. A schematic of the optically-accessible engine, including a dimensionally-accurate representation of the bowl geometry, is shown in Fig. 1. In this optical engine, the geometric compression ratio is 13.75—somewhat lower than the target of 16 typical of low-temperature combustion systems due to the large top ring land required for side-view imaging. The optical engine also features a swirl control valve, which was operated in a position providing a swirl ratio of 2.6.

The operating condition selected employed an EGR rate of 56%, corresponding to an O_2 mole fraction of 0.12. A suite of emissions measurements demonstrated that, at the selected speed and load, this intake O_2 level corresponds to the threshold of a large increase in soot and CO. Thus, the spatial distributions of partially-burned fuel and

particulate measured here are those existing at the practical dilution-limit of this combustion system. To permit optical detection of combustion intermediates, a non-fluorescing fuel mixture of 70% n-heptane and 30% iso-octane (with a small amount of lubricity improver) was used. This mixture has an estimated cetane number of 45 and a density of 85% that of Swedish diesel fuel.

Interfacing with the 8 Hz lasers employed in the PIV system required the engine to be operated in a skip-fired mode, whereby fuel was injected on every fifth cycle. Consequently, it was necessary to supply the EGR content of the intake charge from the exhaust of an industrial fuel-oil burner. A second consequence of skip-firing is that the combustion chamber surfaces are cooler, leading to lower TDC temperatures and retarded combustion phasing. To compensate for this effect, a higher intake charge temperature was employed that resulted in approximately the same ignition delay observed when the engine was continuously fired. Additional features of the engine, and of the operating condition at which the measurements were obtained, are tabulated in Table 1.

Although the optical access to the combustion chamber permits the measurement of horizontal plane vector and scalar fields, the results presented below are limited to the vertical plane. For each diagnostic technique a similar experimental configuration was employed, wherein a vertical laser sheet is introduced through the quartz ring comprising the upper cylinder liner (Fig. 1) and light is collected at 90° through the same ring. The camera was positioned such that approximately half the cylinder bore was visible, from the cylinder centerline to the bore wall. For the PIV images, however, scattering and reflections from the quartz ring limited the useful image area to regions further than 3 mm from the bore wall. The 25 mm ring height allows imaging of the full combustion

bowl volume for 35°CA on either side of TDC, and imaging of the squish volume above the piston top for 55°CA. The laser sheet is aligned with the axis of one of the fuel sprays.

The PIV system was based on a 12-bit camera with a 1280 x 1024 sensor, and a pair of frequency-doubled Nd-YAG lasers operated with pulse energies of 50 mJ and an inter-pulse separation of 10 μs. The laser beams are manipulated into sheets characterized by a $1/e^2$ – intensity thickness of 0.25 mm in the region above the piston top. To minimize the impact of luminous soot emissions and other extraneous light sources, the camera was fitted with a 532 nm band-pass interference filter and a mechanical shutter that limited the maximum exposure time to 5-10 ms. Light-scattering particles were introduced with a fluidized bed of bronze beads which was preloaded with porous SiO_2 powder with an average particle diameter of 2.0–2.5 μm. The time constant characterizing the ability of these particles to follow flow velocity changes is about 15 μs at the thermodynamic conditions prevailing near TDC.

Image pairs were processed with an adaptive multi-pass algorithm, finishing with a 32 x 32 pixel interrogation window and a 50% overlap. With these parameters, and a spatial resolution of 32 μm/pixel, vectors are computed approximately every 0.5 mm. False vectors are removed by applying a 2-σ median filter and the mean vector fields are based on 100 single-cycle realizations. For presentation purposes, only every other vector is shown. For the vector-field divergence analysis, all available vectors are employed. To compute the divergence, the mean vector fields are smoothed by convolution with a σ = 1.0 mm Gaussian filter kernel, and the velocity gradients are estimated by first-order differencing. A continuous field is generated by interpolating linearly between vector locations.

LIF images of unburned hydrocarbons are obtained with 120 mJ of laser excitation energy at 355 nm, focused to a sheet thickness of roughly 0.5 mm within the cylinder. Elastically-scattered light is eliminated using a combination of two Schott GG385 and one GG395 long-pass filters to restrict collection to wavelengths greater than 400 nm. The resulting signal will thus have components from a variety of sources, including both H_2CO fluorescence [4] and PAH fluorescence [8]. Both of these sources can be considered to originate from partially-oxidized fuel fragments. Note that the parent fuel blend exhibits no fluorescence when excited with 355 nm light.

LII measurements of the spatial distribution of soot were performed with a 1064 nm laser source operating at 80 mJ per pulse. At this power level, and a focused sheet thickness of near 0.5 mm, the laser sheet fluence within the cylinder was maintained near 0.6 J/cm^2—well within the LII plateau region. The LII signal was short-pass filtered at a cut-off wavelength of 450 nm, and an additional, heat absorbing Schott filter (KG3) was employed to further attenuate light beyond 600 nm.

Both the LIF and LII signals were integrated on an ICCD camera for a period of 100 ns beginning 10 ns before the laser pulse. At each crank angle 50 images were acquired.

Because the curved combustion chamber walls induce significant optical distortion, a correction must be applied to obtain accurate vector fields from the raw PIV images. The distortion correction was performed by fitting a two-dimensional cubic polynomial to a matrix of points on the distorted image of a target placed within the combustion chamber. An example of a distorted target image, and its distortion-corrected counterpart, is shown in Fig. 2. The most important feature to note is that roughly the

upper 50% of the "bowl" region in the distorted image shows significant distortion and blurring. By comparison with the corrected image, however, we see that this blurred region corresponds to a relatively small region less than 1 mm below the piston top. In contrast, the lower 50% of the distorted "bowl" region remains relatively well focused, and in the corrected image is seen to contain information to within 1 mm of the piston top. Accordingly, a nearly complete view of the bowl region is contained in the lower portion of the distorted image, due to the beneficial lensing effect of the curved bowl side walls. Note, though, that the squish region, which suffers from relatively little distortion in the raw image, is highly distorted in the corrected image. The full distortion-corrected image is thus obtained by separately correcting (and post-processing) the bowl region and the squish region, and subsequently pasting the relevant regions together in a collage. A similar correction is also used to eliminate ambiguities in the LIF and LII images, though the full distortion correction has not been employed.

3. Mean Field Results

To place the development of the measured velocity, partially-oxidized hydrocarbons, and soot distributions at each crank angle in proper context, the mean rate of apparent heat release and the corresponding integrated, cumulative heat release measured at the selected operating condition are shown in Fig. 3. During the period following injection, when the heat release rate is negative, the LIF images show little evidence of partially-oxidized fuel (POF)—as is indicated by the mean image obtained at -5° shown in the upper portion of Fig. 4. By -3°, however, POF is clearly observed in the central region of the bowl, where it marks the location of the low-temperature heat release seen in Fig. 3 at this time.

As the combustion proceeds to the onset of the main heat release near TDC, POF is found chiefly in the upper regions of the cylinder, corresponding roughly to the path of the fuel spray. At this time, the first valid velocity fields are obtained (at earlier times, elastic scattering from the fuel spray saturates the PIV images). The mean velocity field at TDC, shown in the lower portion of Fig. 4, is dominated by a single vortical structure characterized by velocities of 2–3 times the mean piston speed S_p near the vortex periphery. This structure, generated by the deflection of the radial spray momentum at the bowl wall, will transport fluid over distances of approximately 4–6 mm in a 4° period. Considering the location of this vortical structure, and the relative locations of the POF seen at -3° and at 1°, it is likely that a portion of the POF fluorescence seen at TDC originates from POF which has been transported upward from the central region of the bowl.

Numerical simulations show that an approximate degree of axisymmetry is achieved relatively shortly after the end of injection. Accordingly, the divergence $\nabla \cdot \overline{\mathbf{U}}$ can be estimated from the two-dimensional velocity fields of Fig. 4, and is depicted as a false-color background. The divergence can be physically interpreted as the normalized rate of expansion of a fluid element of volume V—$(1/V)(dV/dt)$. Regions of large positive divergence are thus expected to correlate well with regions of heat release. With this perspective, the divergence observed near TDC is in good qualitative agreement with the distribution of POF. Both diagnostics suggest that a significant fraction of the initial heat release takes place in the upper region of the bowl, although the divergence indicates that additional heat release also occurs lower in the bowl.

This lower region of heat release is confirmed by the POF images obtained shortly thereafter, where by 5° intense POF fluorescence is observed in the central region of the bowl. This fluorescence dissipates very rapidly, and has nearly vanished just 2° later. In light of the rapidly increasing heat release rate seen in Fig. 3at this time, we believe the rapid dissipation is caused by the onset of high-temperature reactions that rapidly consume the fluorescing combustion intermediates. This interpretation is also consistent with the main region of heat release indicated by $\nabla \cdot \overline{\mathbf{U}}$ estimated at 5°. The rapid dissipation could also be caused by out-of-plane transport of the POF by the swirl velocity. However, images of natural luminosity taken through the extended piston (not presented here) reveal a fairly uniform azimuthal intensity distribution—suggesting this is not a significant factor.

Figure 5 shows the distributions of soot LII, POF fluorescence, and flow velocity measured in the period corresponding to the latter portion of the main heat release and the early portion of the mixing-controlled burn period. The first indications of laser-induced soot incandescence are observed at 10–11° near the cylinder centerline and, to a lesser extent, near the bowl rim. Because temperatures greater than approximately 1700 K are required to form soot on engine time-scales [2], the delayed appearance of soot until after significant heat release has occurred is consistent with both expected behavior and with observations in large-bore engines [5]. The initial distributions of soot are closely mirrored by the distributions of POF—two dominant regions, one near the centerline and the other near the bowl lip, are observed. As the cycle progresses, however, little soot is observed outside the centerline region. Soot is formed in regions characterized by a mixture fraction greater than approximately twice the stoichiometric value f_{stoich}. Hence,

the intense LII signal from this region indicates that a significant fraction of the mixture in this region is fuel rich.

POF fluorescence is also observed from the squish region at the latter crank angles displayed in Fig. 5, and could emanate from either the products of fuel-rich combustion or from the partial oxidation of fuel-lean mixtures. With operation at a global λ of 1.15, however, the existence of sufficiently lean mixtures over a large portion of the combustion chamber seems unlikely. Additionally, some indication of soot incandescence is also seen here. Overall, it is likely that the squish region fluorescence is also associated with partially-oxidized products of fuel rich combustion, although the average mixture composition is undoubtedly leaner than near the cylinder centerline. To better distinguish between these two cases, identification of the spectral characteristics of H_2CO in the POF fluorescence may prove useful [4].

During this period, the clockwise-rotating vortical structure that dominated the earlier flow field evolves into a counter-rotating structure. The dominant heat release zones indicated by the flow divergence estimates are observed in the upper-central bowl region, near the lower portion of the centerline region of intense soot incandescence and POF fluorescence. The vortical structure dominating the flow is positioned such that, on average, the fluid in this heat release zone and the POF near the cylinder centerline is either recirculated or extended axially as the piston descends—there is little mean flow motion that could transport this fluid to the outer regions of the cylinder.

Vector fields outside of the bowl are first obtained at 15°, and reveal a second region of high flow divergence near the edge of the bowl, adjacent to the squish volume region exhibiting POF fluorescence. We do not believe this flow divergence is associated

with heat release, as a similar region is observed at this crank angle when no fuel is injected. Rather, a lack of flow axisymmetry due to the protrusion of the pressure transducer from the head is the likely source. Beyond 15°, the variations in divergence observed within the squish volume are comparable to the variations observed with no fuel injection, and should not be interpreted to indicate zones of mean heat release. Finally, like the centerline region, beyond 15° there is little mean flow motion in the squish region from which POF fluorescence is observed, other than axial straining. Consequently, the fluorescence is emanating from fluid that was deposited there earlier in the cycle.

Much of the behavior observed at the latter crank angles shown in Figure 5 carries through to the late-cycle period of combustion depicted in Figure 6. Numerical simulations [9] and experimental studies [10] show that, for conventional diesel combustion regimes, a significant fraction of soot oxidation occurs during this period. However, for this modified engine design and low-temperature operating condition, the measurements are indicative of poor late-cycle oxidation performance. Images of soot incandescence show that the soot distribution remains concentrated along the cylinder centerline, as does the bulk of the fluid from which POF fluorescence is observed. Similarly, the spatial distribution of POF fluorescence from the squish volume does not vary significantly. Both regions simply elongate axially, while slowly spreading radially. By 63°, the two regions of POF fluorescence blend together smoothly—suggesting that, on average, the unutilized O_2 in the cylinder is found exclusively in the outer periphery of the squish volume.

The mean flow structures shown in Fig.6 are fully consistent with the evolution of the soot and POF distributions. The flow field in the squish volume and near the cylinder centerline is characterized by very little radial motion. The largest radial velocities are found near the bowl lip ($r \approx 2$–3 cm). However, for a typical radial velocity near 2 ms^{-1}, fluid in this region will be displaced by less than 1 cm during the 30° period shown in Fig. 6. Consequently, very little bulk transport of soot and POF by mean flow structures, other than axial extension, occurs anywhere in the cylinder.

4. Single-Cycle Results

A key remaining question is whether or not the measured flow fields and spatial distributions of soot and POF observed in the mean fields presented in Figs.4–6 are representative of the fields that exist on a single-cycle basis. To address this question, single-cycle realizations are examined at a crank angle near 30° in Fig. 7. Representative flow fields and images of soot incandescence and POF fluorescence have been selected to demonstrate the range of variation observed in the single-cycle images. From the soot images in the upper portion of Fig. 7, it is apparent that on any given cycle the soot distribution near the cylinder centerline can vary significantly. POF fluorescence near the centerline exhibits a similar variability from cycle-to-cycle, but additionally marks POF in the squish region. Hence, the dual-zone POF distributions exhibited in the averaged images are clearly present in individual cycles, and do not result from averaging over distinct realizations exhibiting POF in only one zone at a time.

The individual flow fields display a remarkable similarity to the mean flow field shown in Fig. 6. The flow within the bowl, upon high-pass filtering, clearly exhibits turbulent eddies. However, the dominant flow component is associated with the piston-

induced motion, and turbulent transport of species in the bowl will be small as compared to the axial mean flow transport. Likewise, elements of the mean flow (e.g. the looping structure above the bowl lip and the structure within the squish volume) also dominate portions of the single-cycle flow fields observed outside the bowl. Only in the upper-central region of the chamber is significant variability in the large-scale flow structures observed—variability that is likely linked to variability in the locations of heat release caused by cycle-to-cycle changes in the distributions of POF and soot in the same region.

5. Summary and Conclusions

Measurement of vertical-plane velocity fields and of the spatial distributions of partially-oxidized fuel and soot allow the progress of the combustion process to be examined on a detailed level that is critical for validating predictions of numerical simulations and for developing a phenomenological understanding of the factors responsible for high emissions or fuel consumption. These measurements have been obtained in a swirl-supported, direct-injection diesel engine for a highly-dilute, low-temperature operating condition, and are employed to follow the evolution of the combustion process from shortly after injection until late in the expansion stroke.

The initial distributions of partially-oxidized fuel are found to correlate well with regions of heat release identified from estimates of the mean velocity field divergence. Later in the cycle, soot observed in the central region of the cylinder is found to be spatially-coincident with partially-oxidized fuel. Soot in this region is not readily oxidized, nor do mean flow structures exist that readily transport it to other regions of the cylinder. Within the squish volume little soot is found, although partially-oxidized fuel is clearly observed. Fluid from this region, though not a dominant source of soot emissions,

may contribute substantially to unburned hydrocarbon or CO emissions due to the large volume occupied.

Single-cycle measurements of flow structures and of soot and partially-oxidized fuel distributions show remarkable similarity to the mean measurements, and lend support to the continued use of RANS-based models for the design and optimization of these engines.

Acknowledgements

This research was performed at the Lund Institute of Technology and at the Combustion Research Facility of Sandia National Laboratories. The authors gratefully acknowledge the Swedish Energy Agency and the US Department of Energy, Office of FreedomCar and Vehicle Technology, for their support.

References

1. S. Kimura, H. Ogawa., Y. Matsui, Y. Enomoto, *Int'l. J. Engine Res.* 3 (4) (2002) 249-259.
2. K. Akihama, Y. Takatori, K. Inagaki, S. Sasaki, A.M. Dean, *Trans. SAE: J. of Engines* 110 (2001) Paper 2001-01-0655.
3. P.C. Miles, in C. Arcoumanis (Ed.) *Flow and Combustion in Automotive Engines*, Springer-Verlag. *In Press*
4. T. LaChaux, M.P.B. Musculus, *Submitted to Proc. Combustion Inst.* 31.
5. J.E. Dec, C. Espey, *Trans. SAE: J. of Engines* 104 (1995) Paper 950456.
6. G. Särner, M. Richter, M. Aldén, L.Hildingsson, A. Hultqvist, B.Johansson, *SAE Technical Paper* 2005-01-3869 (2005).

7. W.S. Mathews, T. Fang, R.E. Coverdill, C.-F. Lee, R.A. White, *SAE Technical Paper* 2004-01-1412 (2004).
8. J.T. Kashdan, N. Docquier, G. Bruneaux, *Trans. SAE: J. of Fuels and Lubricants* 113 (2004) Paper 2004-01-2945.
9. Y. Liu, A. Amr, R.D. Reitz, *Trans. SAE: J. of Engines* 113 (2004) Paper 2004-01-0105.
10. X. Li, J.S. Wallace, *Trans. SAE: J. of Engines* 104 (1995) Paper 950848.

Table 1
Engine features and operating parameters

Fuel injection:	Bosch common-rail
Nozzle:	5-hole VCO
	360 cm^3/30 s
Rail pressure:	750 bar
Injection timing:	-12.5°
Intake temperature, T_{in}:	83 °C
Skip-fired T_{in}:	125 °C
Intake pressure:	1.1 bar
Intake O_2 :	12 vol.%
Engine speed:	1200 RPM
Mean piston speed, S_p	3.73 ms^{-1}
Load (IMEP):	4 bar
Lambda:	1.15

List of Figure Captions:

Figure 1. Schematic view of the optically accessible Volvo D5 and the experimental set-up

Figure 2. Illustration of a distorted image and the result of applying a distortion correction within the bowl region. The overlay on the corrected image is the original grid employed to generate the target

Figure 3. The apparent heat release rate and the cumulative heat release derived from in-cylinder pressure measurements

Figure 4. Averaged images of partially-oxidized fuel and vertical-plane mean flow fields measured during the initial stages of the combustion process. To avoid difficulties with the term $(1/r)\,\partial(r\overline{U_r})/\partial r$, the flow divergence shown in the false-color background of the vector fields has been set to zero for $r < 3$ mm

Figure 5. Mean flow structures and averaged spatial-distributions of soot and partially-oxidized fuel measured in the latter half of the main heat release and in the initial stages of mixing-controlled burning

Figure 6. Late-cycle mean and averaged spatial-distributions of soot and partially-oxidized fuel. In this period the velocity field divergence did not differ significantly from that observed without fuel injection, and hence is not reported

Figure 7. Single-cycle images of soot, partially-oxidized fuel, and vertical plane flow structures. The flow fields have been spatially-filtered using a Gaussian kernel with σ = 1.0 mm

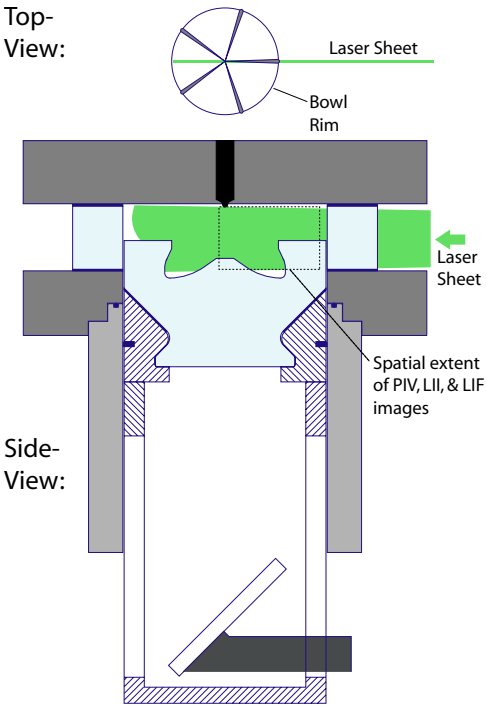

Figure 1. Schematic view of the optically accessible Volvo D5 and the experimental set-up

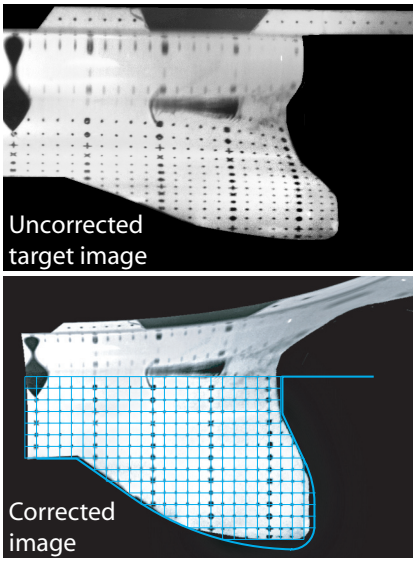

Figure 2. Illustration of a distorted image and the result of applying a distortion correction within the bowl region. The overlay on the corrected image is the original grid employed to generate the target

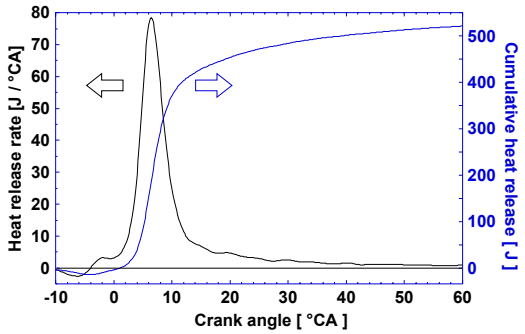

Figure 3. The apparent heat release rate and the cumulative heat release derived from in-cylinder pressure measurements

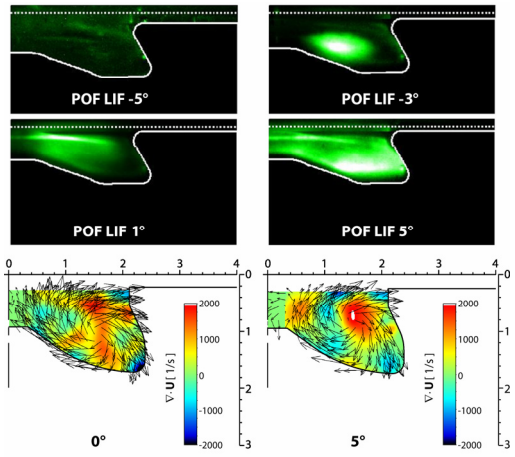

Figure 4. Averaged images of partially-oxidized fuel and vertical-plane mean flow fields measured during the initial stages of the combustion process. To avoid difficulties with the term $(1/r)\partial(r\overline{U}_r)/\partial r$, the flow divergence shown in the false-color background of the vector fields has been set to zero for $r < 3$ mm

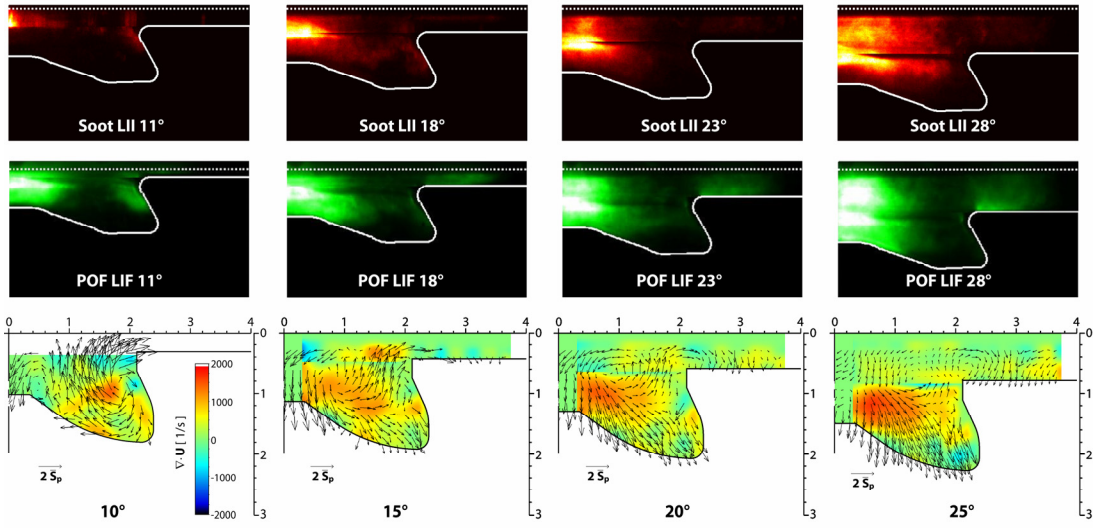

Figure 5. Mean flow structures and averaged spatial-distributions of soot and partially-oxidized fuel measured in the latter half of the main heat release and in the initial stages of mixing-controlled burning

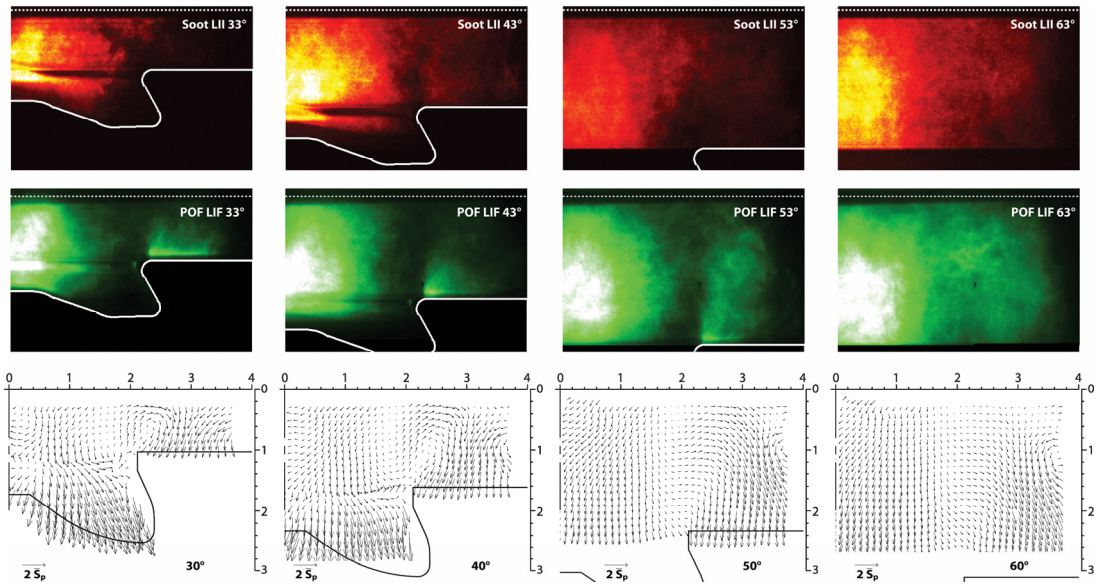

Figure 6. Late-cycle mean and averaged spatial-distributions of soot and partially-oxidized fuel. In this period the velocity field divergence did not differ significantly from that observed without fuel injection, and hence is not reported

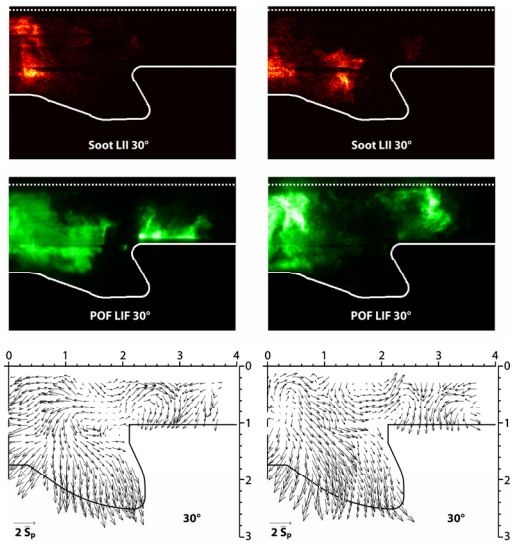

Figure 7. Single-cycle images of soot, partially-oxidized fuel, and vertical plane flow structures. The flow fields have been spatially-filtered using a Gaussian kernel with σ = 1.0 mm